Assessment of Biologic Aggressiveness of Prostate Cancer: Correlation of MR Signal Intensity with Gleason Grade after Radical Prostatectomy[1]

Liang Wang, MD, PhD
Yousef Mazaheri, PhD
Jingbo Zhang, MD
Nicole M. Ishill, MD
Kentaro Kuroiwa, MD[2]
Hedvig Hricak, MD, PhD

Purpose: To retrospectively investigate whether the signal intensity (SI) of prostate cancer on T2-weighted magnetic resonance (MR) images correlates with the Gleason grade at whole-mount step-section pathologic evaluation after radical prostatectomy.

Materials and Methods: The institutional review board approved and issued a waiver of informed consent for this HIPAA-compliant study of 74 patients (median age, 57.5 years; range, 32–72 years) who underwent endorectal MR imaging before radical prostatectomy, with subsequent whole-mount step-section pathologic evaluation, between January 2001 and July 2004. Inclusion criteria were that they had: no prior treatment; at least one lesion of uniform Gleason grade 3 or 4 or with Gleason grade 5 components, with a bidimensional diameter product of 20 mm^2 or greater; no high SI on T1-weighted MR images indicative of postbiopsy changes; and an interval of more than 4 weeks between biopsy and MR imaging. SI of prostate tumors, nontumor prostatic tissue, and internal obturator muscles was measured on uncorrected and corrected T2-weighted MR images. Correlations between Gleason grades and SI ratios were assessed by using generalized estimating equations. SI ratios in peripheral zone (PZ) and transition zone (TZ) lesions of the same Gleason grade were compared with an unpaired *t* test.

Results: Seventy-nine Gleason grade 3, eight Gleason grade 4, and four mixed Gleason grades 4 and 5 lesions identified at pathologic evaluation were analyzed. Gleason grade correlated significantly with tumor-muscle SI ratio for PZ tumors on corrected and uncorrected images ($P = .006$ and $<.001$, respectively). Higher Gleason grades were associated with lower tumor-muscle SI ratios. Nontumor-muscle SI ratios did not correlate with patients' Gleason grades. Tumor-muscle SI ratios were lower in TZ than in PZ tumors ($P < .001$).

Conclusion: Higher Gleason grades were associated with lower tumor-muscle SI ratios on T2-weighted MR images. SI evaluation on T2-weighted MR images may facilitate noninvasive assessment of prostate cancer aggressiveness.

[1] From the Departments of Radiology (L.W., Y.M., J.Z., H.H.), Medical Physics (Y.M.), Epidemiology and Biostatistics (N.M.I.), and Urology (K.K.), Memorial Sloan-Kettering Cancer Center, 1275 York Ave, Rm C-278, New York, NY 10021. Received January 9, 2007; revision requested February 28; revision received May 2; final version accepted June 1. Supported by National Institutes of Health grant R01 CA76423. **Address correspondence to** L.W. (e-mail: *wang6@mskcc.org*).
Current address:
[2] Department of Urology, Graduate School of Medical Sciences, Kyushu University, Fukuoka, Japan.

Prostate cancer is a histologically heterogeneous and frequently multifocal disease (1,2). Its biologic aggressiveness varies greatly and is a key predictor of outcome (2–6). Assessment of the aggressiveness of prostate cancer can help in the stratification of patients for appropriate treatment (1,7).

Since its initial description 40 years ago, the Gleason grading system has been the reference standard for measuring the biological aggressiveness of prostate cancer (8–10). Gleason grades range from 1 to 5, indicating gradations from well to poorly differentiated prostate cancer, respectively. When the pathologist evaluates tumor aggressiveness, he or she assigns both a primary and a secondary Gleason grade. The primary grade is the pattern of cancer that is most prevalent; the secondary grade is the pattern of cancer that is the second most prevalent and that accounts for more than 5% of the examined specimen. If no pattern of cancer meets the latter two criteria, the secondary grade is the same as the primary grade. As the Gleason grade increases, the likelihood of disease recurrence becomes greater (8,9,11).

Magnetic resonance (MR) imaging with an endorectal coil is gaining acceptance as a tool for the noninvasive detection, localization, and staging of prostate cancer (1,12,13). It has been established that prostate cancer typically demonstrates lower signal intensity (SI) than nonneoplastic prostate tissue on T2-weighted MR images (14,15). In addition, researchers in one study found that quantitative measurements of SI on T2-weighted MR images, combined with consideration of prostate-specific antigen (PSA) levels, could improve differentiation between benign peripheral zone (PZ) tissue and prostate cancer (16). Although metabolic data from MR spectroscopic imaging has been shown to correlate with Gleason grade (17), to the best of our knowledge, no studies have been done to examine whether SI on MR images might also correlate with Gleason grade. Thus, the purpose of our study was to investigate retrospectively whether the SI of prostate cancer on T2-weighted MR images correlates with the Gleason grade at whole-mount step-section pathologic evaluation after radical prostatectomy.

Advances in Knowledge

- There is a significant correlation between the Gleason grade of prostate cancer and the tumor-muscle signal intensity (SI) ratio on corrected ($P = .006$) and uncorrected ($P < .001$) T2-weighted MR images; a higher Gleason grade is associated with a lower tumor-muscle SI ratio.
- On T2-weighted MR images, cancer of Gleason grade 3 in the transition zone has a significantly lower ($P < .001$) tumor-muscle SI ratio than does cancer of the same grade in the peripheral zone of the prostate.

Materials and Methods

Patients

Between January 2001 and July 2004, 455 patients underwent endorectal MR imaging, followed by radical prostatectomy with subsequent step-section pathologic evaluation. Three hundred eighty-one of these patients were excluded from our study because they did not meet one or more of the following inclusion criteria: no treatment received before radical prostatectomy; at least one tumor of uniform Gleason grade 3 or 4 or with Gleason grade 5 components, with a bidimensional diameter product of 20 mm^2 or greater; no high SI on T1-weighted MR images indicative of changes at the location of prostate cancer on the whole-mount pathologic step-section slices after biopsy; and an interval of more than 4 weeks between biopsy and MR imaging. Thus, a total of 74 patients (median age, 57.5 years; range, 32–72 years; median weight, 86.6 kg; range, 59–125 kg) were included in our study.

Men imaged through June 2003 were part of an ongoing prospective National Institutes of Health study of the use of MR imaging in patients with prostate cancer. All patients gave informed consent before enrollment in the prospective National Institutes of Health study, which was approved by our institutional review board and was compliant with the Health Insurance Portability and Accountability Act. From July 2003 to July 2004, prostate MR imaging occurred as part of clinical practice for patient evaluation. In approving our study, the institutional review board issued a waiver of informed consent for the retrospective review of the results of MR imaging examinations and clinical data for all 455 patients. The median time from biopsy to MR imaging for the 74 patients included in the study was 35 days (range, 32 days before biopsy to 189 days after biopsy), and the median time from MR imaging to surgery was 29 days (range, 1–164 days). In all patients, a tissue diagnosis of prostate cancer was determined with biopsy specimens. Age, weight, serum PSA level, and clinical stage were recorded from the patients' medical records by one of two coauthors (K.K., L.W.).

Implication for Patient Care

- MR imaging may facilitate noninvasive assessment of prostate cancer aggressiveness.

Published online before print
10.1148/radiol.2461070057

Radiology 2008; 246:168–176

Abbreviations:
PSA = prostate-specific antigen
PZ = peripheral zone
ROI = region of interest
SI = signal intensity
TZ = transitional zone

Author contributions:
Guarantor of integrity of entire study, H.H.; study concepts/study design or data acquisition or data analysis/interpretation, all authors; manuscript drafting or manuscript revision for important intellectual content, all authors; manuscript final version approval, all authors; literature research, L.W.; clinical studies, L.W., K.K.; experimental studies, L.W., Y.M.; statistical analysis, N.M.I.; and manuscript editing, L.W., Y.M., J.Z., N.M.I., H.H.

Authors stated no financial relationship to disclose.

MR Imaging Technique and Phantom Study

Endorectal MR imaging was performed with a 1.5-T whole-body MR imager equipped with both a pelvic phased-array coil (GE Medical systems, Milwaukee, Wis) and a commercially available balloon-covered expandable endorectal coil (Medrad, Pittsburgh, Pa) for signal reception. Patients were examined in the supine position. Transverse T1-weighted spin-echo MR images were obtained from the aortic bifurcation to the symphysis pubis by using the following parameters: repetition time msec/echo time msec, 400–700/10–14; section thickness, 5 mm; intersection gap, 1 mm; field of view, 24–26 cm; matrix, 256 × 192; and number of signals acquired, one. Thin-section, high-spatial-resolution transverse, coronal, and sagittal T2-weighted fast spin-echo images of the prostate and seminal vesicles were obtained by using the following parameters: 3650–6917/

Table 1

Patient Characteristics

Characteristic	Value
Clinical data	
Age (y)*	57.5 (37–72)
Weight (kg)*	86.6 (59–125)
PSA before radical prostatectomy (ng/mL)*	5.05 (0.8–76.8)
Tumor clinical stage†	
T1	47 (64)
T2	25 (34)
T3	2 (3)
Tumor pathologic stage†	
T2	58 (78)
T3	15 (20)
T4	1 (1)
Pathologic finding†	
Extraprostatic extension	16 (22)
Seminal vesicle invasion	3 (4)
Lymph node metastasis	4 (5)
Tumor-positive margins	12 (16)

* Data are medians. Numbers in parentheses are ranges.

† Data are numbers of patients (n = 74). Numbers in parentheses are percentages.

Figure 1

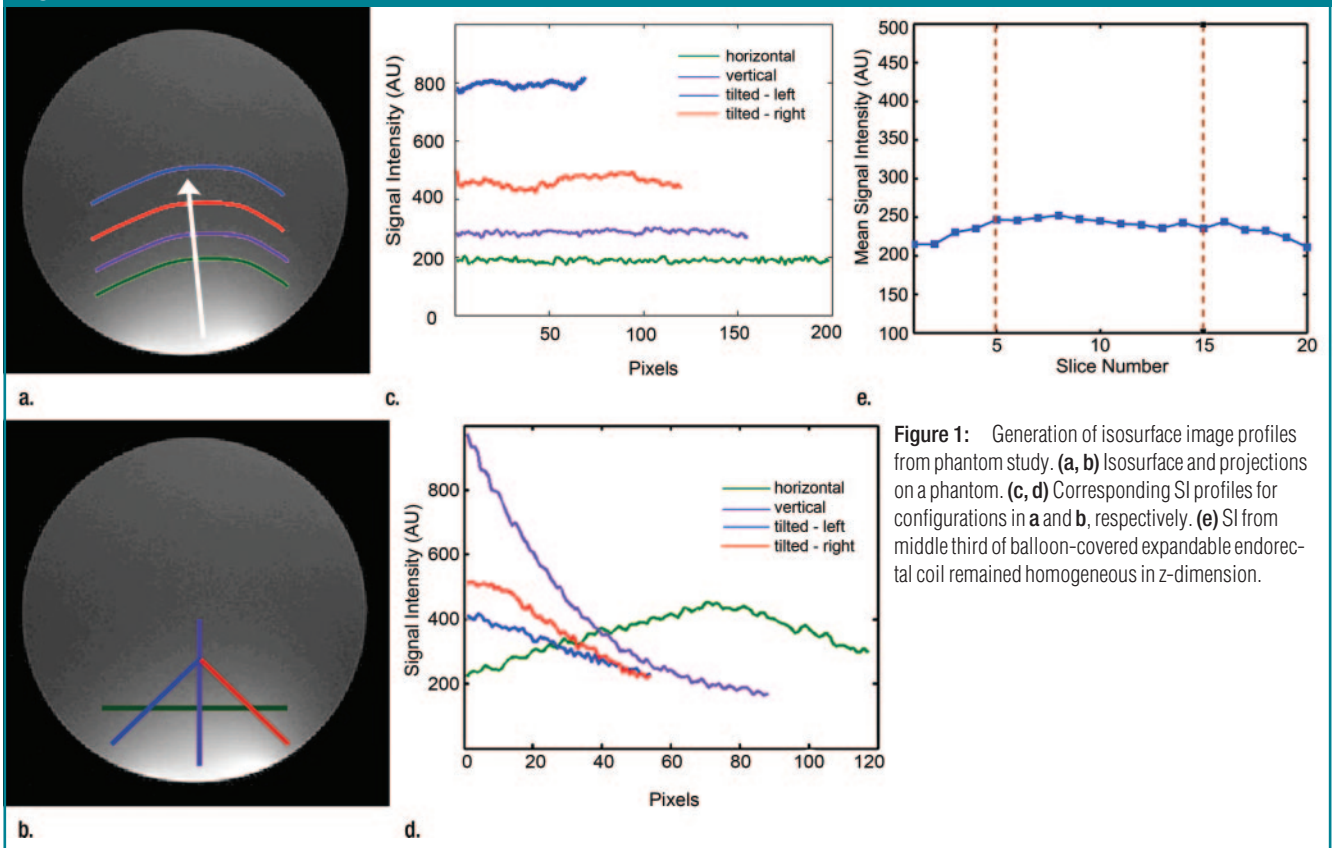

Figure 1: Generation of isosurface image profiles from phantom study. **(a, b)** Isosurface and projections on a phantom. **(c, d)** Corresponding SI profiles for configurations in **a** and **b**, respectively. **(e)** SI from middle third of balloon-covered expandable endorectal coil remained homogeneous in z-dimension.

78–135 (effective); echo train length, 8–32; section thickness, 3 mm; no intersection gap; field of view, 14–20 cm; and matrix, 256–320 × 192. The total time for setup and acquisition was approximately 30 minutes.

Table 2

SI Ratios on Uncorrected and Corrected Images

Image Type and SI Ratio	Value*
Uncorrected images	
Tumor-muscle SI ratio	3.57 (1.22–9.66)
Nontumor-muscle SI ratio	5.93 (1.0–17.6)
Corrected images	
Tumor-muscle SI ratio	2.42 (0.75–8.75)
Nontumor-muscle SI ratio	3.82 (1.79–12.07)

* Data are medians. Numbers in parentheses are ranges.

Table 3

Tumor-Muscle SI Ratios for PZ and TZ Tumors according to Gleason Grade for Uncorrected and Corrected Images

Image Type, Zone, and Gleason Grade	No. of Tumors	Tumor-Muscle SI Ratio*
Uncorrected images		
PZ		
Grade 3	49	5.3 ± 1.65
Grade 4	7	2.9 ± 0.60
Grade 5	3	2.05 ± 0.56
TZ		
Grade 3	30	2.7 ± 0.65
Grade 4	1	1.66†
Grade 5	1	1.22†
Corrected images		
PZ		
Grade 3	49	3.4 ± 1.2
Grade 4	7	1.9 ± 0.40
Grade 5	3	1.2 ± 0.41
TZ		
Grade 3	30	2.1 ± 0.50
Grade 4	1	1.07†
Grade 5	1	0.75†

Note.—For uncorrected images, $P < .001$ for PZ tumors and $P = .13$ for TZ tumors of Gleason grades 3–5. For corrected images, $P = .006$ for PZ tumors and $P = .09$ for TZ tumors of Gleason grades 3–5.

* Data are means ± standard deviations unless otherwise specified.

† Mean value.

Endorectal coil profiles were obtained from a phantom study performed by a medical physicist (Y.M., with 6 years of experience in MR imaging research) and a radiologist (L.W., with 6 years of experience in prostate MR imaging research) to identify the SI isosurface on T2-weighted images. A spheric phantom consisting of saline doped with T1-shortening contrast agent (Magnevist; Berlex, Wayne, NJ) to yield T1 values of approximately 1 second was surrounded with saline bags to mimic the typical conductance of the human prostate and was imaged with the endorectal coil setup. Corrected and uncorrected transverse T2-weighted MR images were generated that were similar to those obtained from a prostate examination. Images were exported to a scientific and engineering software tool (Matlab; MathWorks, Natick, Mass), and SI isosurface profiles were generated both in the z-direction and, as a function of distance to the endorectal coil, in the in-plane direction on T2-weighted MR images.

Image postprocessing was performed with prostatic analytic coil correction software (GE Medical Systems) on the transverse T1- and T2-weighted MR images to correct for the reception profile of the endorectal and external pelvic phased-array coils. All MR imaging data were transferred to the picture archiving and communication system (GE Medical Systems) of our radiology department.

Pathologic Evaluation

After prostate resection, the specimen was step-sectioned into 3–5-mm slices, as previously described (18) and reviewed by a urologist (K.K., with 4 years of experience in uropathology) who was not aware of the MR imaging findings. Cancer foci were outlined in ink on whole-mount apical and seminal vesicle slices so as to be grossly visible and were then photographed to provide tumor maps. The greatest diameter and the greatest perpendicular diameter for each lesion on the whole-mount step-section maps were measured, and bidimensional products were calculated. The locations of tumors were recorded for the PZ or the transition zone (TZ) and the base, middle, or apex of the prostate. The pathologic stage and the presence of extraprostatic extension, seminal vesicle invasion, lymph node metastasis, and tumor-positive margins also were recorded.

MR Image Analysis

MR images and whole-mount pathologic step-section slices were analyzed in consensus by a radiologist (L.W.) and a urologist (K.K.). The radiologist was blinded to the Gleason grade but knew the location of the lesion from the whole-mount step-section pathologic maps, which were printed in black and white with each tumor area outlined in black. The whole-mount pathologic step-section slices were matched with the most closely corresponding T2-weighted MR images.

Tumors that had a bidimensional diameter product of 20 mm^2 or greater on whole-mount pathologic maps and that were of uniform Gleason grade 3 or 4 or contained Gleason grade 5 components were analyzed; if a patient had more than one such tumor, the two largest tumors were analyzed. On both corrected and uncorrected transverse T2-weighted images, by using the pathologic maps as a guide, the radiologist (L.W.) drew a region of interest (ROI) in the center of each tumor. He began by locating a voxel in the center of the tumor with the help of the cross-referencing feature of the picture archiving and communication system, which automatically displays a voxel that is selected in one plane in the two intersecting planes as well. He then drew a round or elliptic (approximately round) ROI around the selected voxel in the transverse plane. To ensure that tumor edges would not be included, he drew the ROI so that its short axis was approximately half the length of the greatest perpendicular diameter of the lesion as seen on the transverse image (ROI area range, 4–10 mm^2).

When a tumor extended through both the PZ and the TZ, two separate ROIs, one in the PZ and one in the TZ

Figure 2

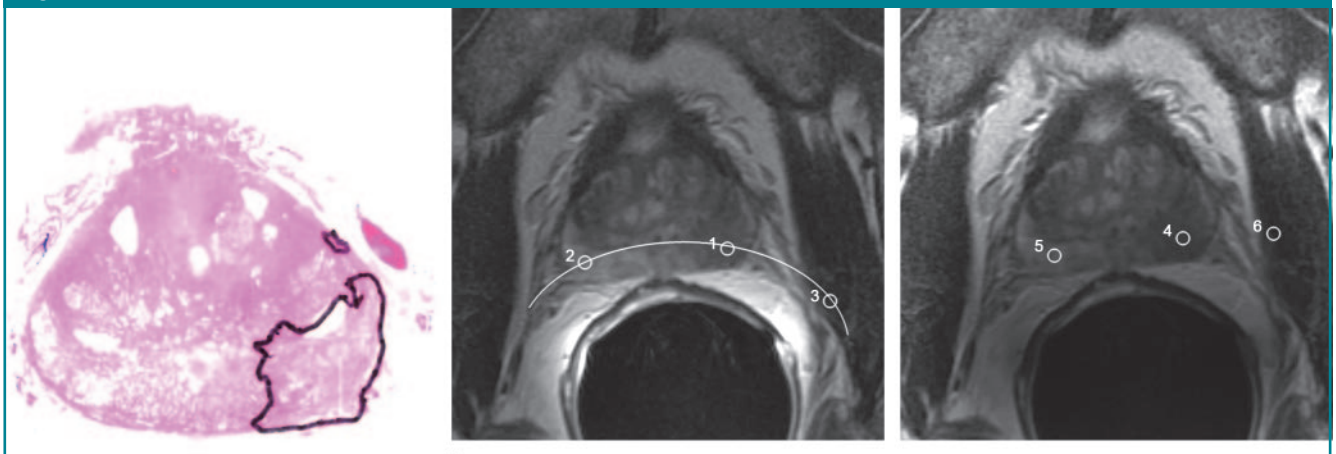

a. b. c.

Figure 2: Prostate cancer in PZ (Gleason grade 4) in 54-year-old man (weight, 100.2 kg; PSA level, 4.4 ng/mL; tumor, clinical stage T2b and pathologic stage T3b). **(a)** Whole-mount step-section pathologic tumor map shows index lesion of Gleason grade 4 in left PZ. Black outlined area represents the area of Gleason grade 4. **(b)** On the corresponding transverse uncorrected T2-weighted MR image (4916.7/102.48; echo train length, 12; field of view, 14 cm; section thickness, 3 mm; no intersection gap), ROIs were placed on center of tumor *(1)*, on nontumor prostatic tissue *(2)*, and on internal obturator muscle *(3)*. PZ tumor-muscle SI ratio was 2.27. PZ nontumor prostatic tissue-muscle SI ratio was 4.86. **(c)** On corresponding transverse T2-weighted MR image corrected with prostatic analytical coil correction software, ROIs were placed on center of tumor *(4)*, on contralateral nontumor prostatic tissue *(5)*, and on internal obturator muscle *(6)*. PZ tumor-muscle SI ratio was 1.82. The PZ nontumor prostatic tissue-muscle SI ratio was 3.44.

portion of the tumor, were placed. The ROIs were placed so as not to include the prostate capsule or urethra. Mean SI values and standard deviations in the ROI were automatically calculated by the picture archiving and communication system. For normalization, ROI measurements in nontumor prostatic tissue and the internal obturator muscle were performed on both corrected and uncorrected images.

To correct for SI inhomogeneity from the endorectal coil, two approaches were used for evaluating SI values on corrected and uncorrected images. On uncorrected T2-weighted transverse images, the mapped isosurface profile obtained from the phantom study was used to guide ROI selection. Round or elliptic ROIs (area range, 4–10 mm^2) were placed on nontumor prostatic tissue and internal obturator muscle along the SI isosurface of the tumor ROI. On T2-weighted transverse MR images corrected with prostatic analytic coil correction software, ROIs were placed on contralateral nontumor

Figure 3

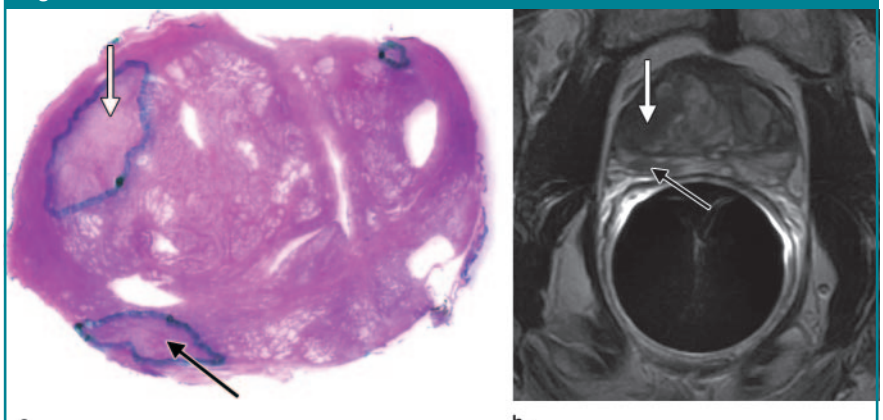

a. b.

Figure 3: Prostate cancers in PZ and TZ (Gleason grade 3) in 60-year-old man (weight, 80.7 kg; PSA level, 5.1 ng/mL; tumor, clinical stage T2b and pathologic stage T2c). **(a)** Whole-mount step-section pathologic tumor map shows index lesion of Gleason grade 3 in right TZ (white arrow) and a second dominant lesion of same grade in the right posterior PZ (black arrow). Outlined areas represent the tumors. **(b)** Corresponding transverse T2-weighted MR image (4000/103 [effective]; echo train length, 16; field of view, 14 cm; acquisition matrix, 256 × 192; section thickness, 3 mm; no section gap) corrected with prostatic analytic coil correction software shows index lesion of Gleason grade 3 in TZ (white arrow) and second dominant lesion of same grade in PZ (black arrow). Tumor-muscle SI ratio of 1.77 in TZ was lower than that of 3.99 in PZ. PZ tumor-muscle SI ratio of 3.99 in this lesion of Gleason grade 3 was higher than SI ratio of 1.82 for lesion of Gleason grade 4 in different patient shown in Figure 2.

prostatic tissue symmetrically to the tumor ROI and on internal obturator muscle as close to the tumor as possible (distance range, 6–28 mm). The mean SI values of the ROIs were used to calculate the tumor-muscle and nontumor-muscle SI ratios.

Statistical Analysis

On both the uncorrected and corrected images, generalized estimating equations with robust sandwich variance estimates and an independence working correlation matrix were used to examine correlations between Gleason grades and tumor-muscle and nontumor-muscle SI ratios, accounting for the clustering caused by patients who contributed more than one lesion. An unpaired *t* test was used to test for differences in tumor-muscle and nontumor-muscle SI ratios between PZ and TZ lesions of the same Gleason grade. In all statistical methods, a *P* value of less than .05 was considered to indicate a significant difference. Analyses were performed with statistical software (Intercooled Stata 8.0 for Windows, 2003, Stata, College Station, Tex; SAS for Windows 9.0, 2002, SAS Institute, Cary, NC).

Results

Patient and Lesion Characteristics, Phantom Study, and SI Ratios

Seventy-four patients with a total of 91 lesions were included in the study (Table 1). At histopathologic examination, 17 patients each had two lesions analyzed. Of 91 lesions, 59 (65%) were in the PZ and 32 (35%) were in the TZ. The Gleason grade classification was as follows: 79 (87%), grade 3; eight (9%), grade 4; and four (4%), mixed grades 4 and 5. At whole-mount step-section pathologic evaluation, the median lesion diameter was 16 mm (range, 5–48 mm), the median greatest perpendicular diameter was 8 mm (range, 4–38 mm), and the median bidimensional product was 144 mm^2 (range, 20–1824 mm^2). Of 74 patients, 16 (22%) had extracapsular extension, three (4%) had seminal vesicle invasion, and four (5%) had pelvic lymph node metastasis. Figure 1 shows the endorectal profile generated from the phantom study. Table 2 lists the median values and ranges for the SI ratios measured on the uncorrected and corrected images.

Correlation of SI Ratio and Gleason Score

Uncorrected images.—Gleason grade correlated significantly with tumor-muscle SI ratio for PZ tumors ($P < .001$), and tumors with a higher Gleason grade demonstrated lower SI ratios (Table 3, Figs 2–4). The nontumor-muscle SI ratios in the PZ did not differ significantly across patients with different Gleason grades ($P = .4$), and this finding indicated that no significant bias existed in our measurements (Table 3).

Corrected images.—Gleason grade correlated significantly with tumor-muscle SI ratio for PZ tumors ($P = .006$); Gleason grade also correlated with tumor-muscle SI ratio for TZ tumors but not to a significant degree ($P = .09$) (Table 3, Fig 4). In both the PZ and the TZ, tumors with a higher Gleason grade demonstrated lower SI ratios. The nontumor-muscle SI ratios demonstrated no significant difference across patients with tumors of different Gleason grades in the PZ (0.63) or in the TZ ($P = .31$), and this finding indicated that no significant bias existed in our measurements (Table 3).

TZ Tumor versus PZ Tumor

Uncorrected images.—Lesions in the TZ classified as Gleason grade 3 had a significantly lower ($P < .001$) mean tumor-muscle SI ratio than did lesions in the PZ classified as the same grade (Table 3; Figs 3, 4). The numbers of lesions in the TZ classified as Gleason grade 4 and mixed grades 4 and 5 were too small for formal analysis.

Corrected images.—Lesions in the TZ classified as Gleason grade 3 had a

Figure 4

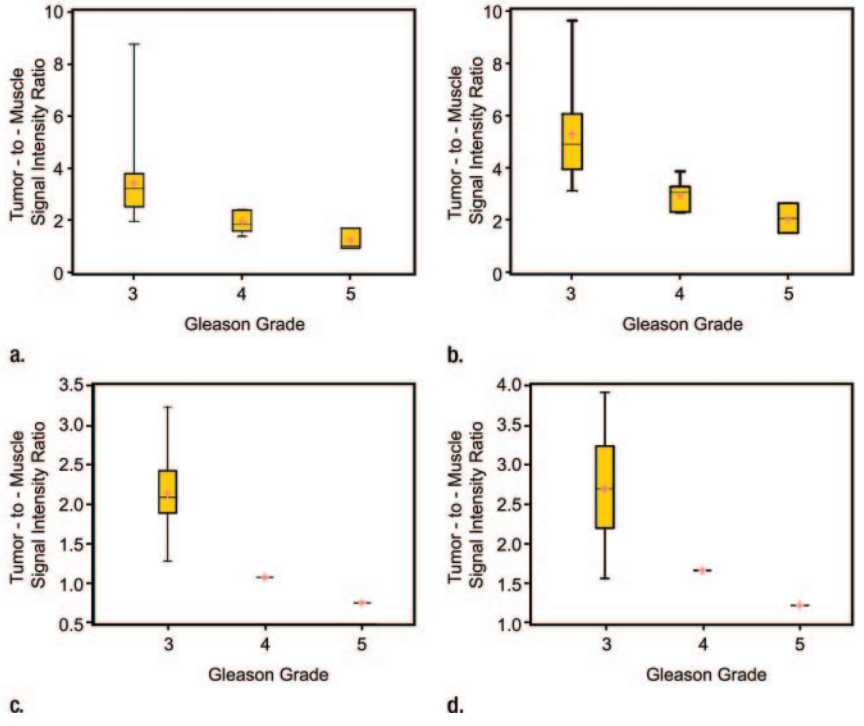

Figure 4: Box plots of tumor-muscle SI ratios on T2-weighted MR images according to Gleason grade of tumors in PZ tumor **(a)** on corrected **(b)** and uncorrected images and in TZ tumor **(c)** on corrected and **(d)** uncorrected images. Red crosses = mean for that group, box = middle 50% of values, black line in box = group median, lines at bottom and top of error bars = minimum and maximum values, respectively.

Table 4

Tumor-Muscle SI Ratios according to Gleason Grade and Location of Tumor for Uncorrected and Corrected Images

Image Type and Tumor Location	Gleason Grade 3		Gleason Grade 4		Gleason Grade 5	
	No. of Lesions	Tumor-Muscle SI Ratio*	No. of Lesions	Tumor-Muscle SI Ratio*	No. of Lesions	Tumor-Muscle SI Ratio*
Uncorrected images						
PZ						
Apex	21	5.6 ± 1.5	4	2.7 ± 0.46	0	. . .
Middle	25	5.3 ± 1.8	1	3.9†	1	2.6†
Base	3	3.8 ± 0.75	2	2.8 ± 0.69	2	1.8 ± 0.39
TZ						
Apex	5	2.75 ± 0.76	1	1.66†	0	. . .
Middle	24	2.7 ± 0.66	0	. . .	0	. . .
Base	1	2.5†	0	. . .	1	1.22†
Corrected images						
PZ						
Apex	21	3.4 ± 0.96	4	1.8 ± 0.45	0	. . .
Middle	25	3.5 ± 1.5	1	2.4†	1	1.7†
Base	3	2.6 ± 0.18	2	2.0 ± 0.22	2	0.96 ± 0.05
TZ						
Apex	5	2.5 ± 0.74	1	1.07†	0	. . .
Middle	24	2.0 ± 0.42	0	. . .	0	. . .
Base	1	2.1†	0	. . .	1	0.75†

* Data are means ± standard deviations unless otherwise specified.

† Mean value.

significantly lower ($P < .001$) mean tumor-muscle SI ratio than did lesions in the PZ classified as the same grade (Table 3; Figs 3, 4).

Basal Tumor versus Middle Tumor versus Apical Tumor

Uncorrected images.—Most of the tumors classified as Gleason grade 3 were in the middle and apex of the prostate. For these two regions, the mean tumor-muscle SI ratios of lesions classified as Gleason grade 3 did not differ significantly ($P > .05$) (Table 4). The numbers of tumors classified as Gleason grade 4 and mixed grades 4 and 5 were too small for formal analysis.

Corrected images.—The mean tumor-muscle SI ratios for lesions classified as Gleason grade 3 did not differ significantly ($P > .05$) for those in the middle and the apex of the prostate (Table 4).

Discussion

Endorectal MR imaging, with and without MR spectroscopic imaging, has the capacity to aid in the detection, localization, and staging of prostate cancer (19–24). Furthermore, MR spectroscopic imaging may have a role in the evaluation of tumor aggressiveness, because metabolic data from MR spectroscopic imaging correlate with the Gleason grade of prostate cancer (17). However, to the best of our knowledge, the capacity of MR imaging alone to provide information about tumor aggressiveness has not been explored. Engelhard et al (16) used the SI ratio on T2-weighted MR images and serum PSA level to differentiate benign disease from prostate cancer in the PZ, by using needle biopsy histopathologic findings as the standard of reference. Although their study did not address tumor aggressiveness specifically, findings from it suggested that quantitative evaluation of SI ratios on MR images could provide more information than visual evaluation alone regarding the nature of the tissue in a lesion. Therefore, we decided to investigate whether a correlation existed between SI ratios on T2-weighted MR images and Gleason grades of tumors at whole-mount step-section pathologic evaluation after radical prostatectomy. We found that lower tumor-muscle SI ratios were associated with higher Gleason grades, although there was some overlap between the SI ratios for tumors of different grades, perhaps because of tissue heterogeneity. We also found that, for all lesions classified as Gleason grade 3, mean tumor-muscle SI ratios were significantly lower in the TZ than in the PZ ($P < .001$).

The mechanism underlying our findings is not entirely clear to us. We speculate that the lower SI values in more aggressive tumors may be caused by a higher cellular density. Schiebler et al (25) demonstrated that the SI of prostate lesions on T2-weighted MR images is associated with lesion cellularity, as well as presence and amount of fluid contents, collagen, and fibromuscular stroma. Quint et al (26) and Schiebler et al (25) reported that, histologically, prostate cancer consisted of regions of tightly packed glandular elements with very little open space and high cellular density. The reason that the SI values of

tumors of the same grade are lower for those in the TZ than for those in the PZ could be related to the underlying histologic differences between TZ and PZ tumors (27,28). For example, microscopically, PZ cancer typically contains cubic cells with eosinophilic cytoplasm and vesicular nuclei, whereas TZ cancer often has columnar cells with pale cytoplasm and small dark nuclei (27–29).

The use of an endorectal coil with a phased-array coil substantially increases the signal-to-noise ratio in MR imaging of the prostate and thereby improves tumor detection, localization, and staging (16,30,31). However, it also creates obstacles to the comparison of SI values across patients, since the SI is substantially higher in regions close to the endorectal coil and decreases rapidly with increasing distance from it (32). This SI profile may vary from patient to patient, depending on the orientation of the endorectal coil at insertion. Furthermore, there may be signal variations along the z-axis of the endorectal coil, and the anterior phased-array coil also contributes some signal. For these reasons, SI cannot be compared directly across patients who have undergone MR imaging of the prostate (33). Two approaches may be used to solve this problem: *(a)* Image postprocessing may be implemented to correct for the reception profiles of endorectal and phased-array coils, which is feasible with commercial software. *(b)* An endorectal coil profile may be acquired from a phantom to guide placement of ROIs along a uniform signal profile, referred to as an isosurface. The latter approach does not require image SI correction. Both approaches were used in our study and showed consistent results, indicating that our findings are unlikely to have been influenced by bias. Even though the phantom study showed that SI from the middle third of the endorectal coil remained homogeneous in the z-dimension, we performed all ROI measurements for the tumor, the nontumor prostate tissue, and the internal obturator muscle on the same transverse MR image to minimize potential bias.

Another potential source of error in quantifying prostate cancer is the partial volume effect (34). To prevent the partial volume effect from adjacent nontumor prostatic tissue, only the two largest lesions in the prostate that met the specified size criteria were analyzed. Furthermore, by using the cross-referencing tool of the picture archiving and communication system, ROIs were placed on the centers of tumors to prevent tumor edge effects.

Our analysis was based on Gleason grades assigned at the time of mapmaking, the dates of which preceded the new consensus on Gleason grading. The new consensus document, published in 2005, was largely based on empiric observation rather than on validated data, and, therefore, we did not believe there was a strong need to reevaluate the pathologic samples for our study (10).

Correction of signal nonuniformity when using surface coils in MR imaging is an active area of research (35,36). Several groups have investigated postprocessing methods to minimize the signal nonuniformity of endorectal MR imaging. Some have suggested methods that would not require additional acquisition but would require more advanced algorithms to correct for the bias field effect (32,33,37). Others have proposed methods that require additional data acquisition (36). Our study results suggest that such postprocessing methods have potential clinical utility in the noninvasive assessment of prostate cancer aggressiveness.

One limitation of this study was the exclusion of a number of patients because of technical and clinical issues. Although the median time from biopsy to MR imaging was 35 days, some patients still demonstrated substantial biopsy changes on T1-weighted MR images and corresponding SI loss at T2-weighted MR imaging, which made their data sets unusable. Other limitations were the relatively small numbers of tumors with uniform Gleason grade 4 or with Gleason grade 5 components in the study group; this limitation prevented us from comparing the SI ratios for such tumors in different regions of the prostate.

Another limitation of our study was that the acquisition parameters (repetition time, echo time, echo train length) varied within a very wide range. Such variation could have been a source of error, as it contributes to variation in tumor-muscle SI ratio measurements on T2-weighted MR images among patients.

Our findings suggest that, in addition to providing anatomic information for tumor detection, localization, and staging, T2-weighted endorectal MR imaging may have the potential to allow noninvasive assessment of prostate cancer biological aggressiveness, which could help in the stratification of patients for appropriate treatment. Future studies with larger numbers of patients and prospective quantitative T2 measurement are warranted to confirm our findings.

Acknowledgments: The authors wish to thank Ada Muellner, BA, for editing the manuscript and Carolina Montalvo, BA, and Tamara Torres, BS, for preparing the figures.

References

1. Hricak H. MR imaging and MR spectroscopic imaging in the pre-treatment evaluation of prostate cancer. Br J Radiol 2005;78(Spec no. 2):S103–S111.

2. Ohori M, Kattan M, Scardino PT, Wheeler TM. Radical prostatectomy for carcinoma of the prostate. Mod Pathol 2004;17:349–359.

3. Kattan MW, Wheeler TM, Scardino PT. Postoperative nomogram for disease recurrence after radical prostatectomy for prostate cancer. J Clin Oncol 1999;17:1499–1507.

4. Epstein JI, Partin AW, Sauvageot J, Walsh PC. Prediction of progression following radical prostatectomy: a multivariate analysis of 721 men with long-term follow-up. Am J Surg Pathol 1996;20:286–292.

5. Fryback DG, Albertsen PC, Storer BE. Prostatectomy and survival among men with clinically localized prostate cancer. JAMA 1996; 276:1723–1724.

6. Gerber GS. Reply. JAMA 1996;276:1724.

7. Scardino PT. Continuing refinements in radical prostatectomy: more evidence that technique matters. J Urol 2005;173:338–339.

8. Gleason DF. Classification of prostatic carcinomas. Cancer Chemother Rep 1966;50: 125–128.

9. Gleason DF, Mellinger GT. Prediction of prognosis for prostatic adenocarcinoma by

combined histological grading and clinical staging. J Urol 1974;111:58–64.

10. Epstein JI, Allsbrook WC Jr, Amin MB, Egevad LL. The 2005 International Society of Urological Pathology (ISUP) Consensus Conference on Gleason Grading of Prostatic Carcinoma. Am J Surg Pathol 2005; 29:1228–1242.

11. Epstein JI. What's new in prostate cancer disease assessment in 2006? Curr Opin Urol 2006;16:146–151.

12. Wang L, Mullerad M, Chen HN, et al. Prostate cancer: incremental value of endorectal MR imaging findings for prediction of extracapsular extension. Radiology 2004;232: 133–139.

13. Engelbrecht MR, Jager GJ, Laheij RJ, Verbeek AL, van Lier HJ, Barentsz JO. Local staging of prostate cancer using magnetic resonance imaging: a meta-analysis. Eur Radiol 2002;12:2294–2302.

14. Hricak H, Wang L, Wei DC, et al. The role of preoperative endorectal magnetic resonance imaging in the decision regarding whether to preserve or resect neurovascular bundles during radical retropubic prostatectomy. Cancer 2004;100:2655–2663.

15. Akin O, Hricak H. Imaging of prostate cancer. Radiol Clin North Am 2007;45:207–222.

16. Engelhard K, Hollenbach HP, Deimling M, Kreckel M, Riedl C. Combination of signal intensity measurements of lesions in the peripheral zone of prostate with MRI and serum PSA level for differentiating benign disease from prostate cancer. Eur Radiol 2000; 10:1947–1953.

17. Zakian KL, Sircar K, Hricak H, et al. Correlation of proton MR spectroscopic imaging with Gleason score based on step-section pathologic analysis after radical prostatectomy. Radiology 2005;234:804–814.

18. Yossepowitch O, Sircar K, Scardino PT, et al. Bladder neck involvement in pathological stage pT4 radical prostatectomy specimens is not an independent prognostic factor. J Urol 2002;168:2011–2015.

19. Huzjan R, Sala E, Hricak H. Magnetic resonance imaging and magnetic resonance spectroscopic imaging of prostate cancer. Nat Clin Pract Urol 2005;2:434–442.

20. Wang L, Hricak H, Kattan MW, Chen HN, Scardino PT, Kuroiwa K. Prediction of organ-confined prostate cancer: incremental value of MR imaging and MR spectroscopic imaging to staging nomograms. Radiology 2006;238:597–603.

21. Futterer JJ, Engelbrecht MR, Jager GJ, et al. Prostate cancer: comparison of local staging accuracy of pelvic phased-array coil alone versus integrated endorectal-pelvic phased-array coils—local staging accuracy of prostate cancer using endorectal coil MR imaging. Eur Radiol 2007;17:1055–1065.

22. Wang L, Hricak H, Kattan MW, et al. Prediction of seminal vesicle invasion in prostate cancer: incremental value of adding endorectal MR imaging to the Kattan nomogram. Radiology 2007;242:182–188.

23. Zakian KL, Eberhardt S, Hricak H, et al. Transition zone prostate cancer: metabolic characteristics at 1H MR spectroscopic imaging—initial results. Radiology 2003;229: 241–247.

24. Shukla-Dave A, Hricak H, Eberhardt SC, et al. Chronic prostatitis: MR imaging and 1H MR spectroscopic imaging findings—initial observations. Radiology 2004;231: 717–724.

25. Schiebler ML, McSherry S, Keefe B, et al. Comparison of the digital rectal examination, endorectal ultrasound, and body coil magnetic resonance imaging in the staging of adenocarcinoma of the prostate. Urol Radiol 1991;13:110–118.

26. Quint LE, Van Erp JS, Bland PH, et al. Prostate cancer: correlation of MR images with tissue optical density at pathologic examination. Radiology 1991;179:837–842.

27. Erbersdobler A, Augustin H, Schlomm T, Henke RP. Prostate cancers in the transition zone. 1. Pathological aspects. BJU Int 2004; 94:1221–1225.

28. Augustin H, Erbersdobler A, Hammerer PG, Graefen M, Huland H. Prostate cancers in the transition zone. 2. Clinical aspects. BJU Int 2004;94:1226–1229.

29. McNeal JE, Redwine EA, Freiha FS, Stamey TA. Zonal distribution of prostatic adenocarcinoma: correlation with histologic pattern and direction of spread. Am J Surg Pathol 1988;12:897–906.

30. Hricak H, White S, Vigneron D, et al. Carcinoma of the prostate gland: MR imaging with pelvic phased array coil versus integrated endorectal-pelvic phased-array coils. Radiology 1994;193:703–709.

31. Huch Boni RA, Boner JA, Lutolf UM, Trinkler F, Pestalozzi DM, Krestin GP. Contrast-enhanced endorectal coil MRI in local staging of prostate carcinoma. J Comput Assist Tomogr 1995;19: 232–237.

32. Wald LL, Carvajal L, Moyher SE, et al. Phased array detectors and an automated intensity-correction algorithm for high-resolution MR imaging of the human brain. Magn Reson Med 1995;34:433–439.

33. Moyher SE, Vigneron DB, Nelson SJ. Surface coil MR imaging of the human brain with an analytic reception profile correction. J Magn Reson Imaging 1995;5:139–144.

34. Gonzalez Ballester MA, Zisserman AP, Brady M. Estimation of the partial volume effect in MRI. Med Image Anal 2002;6:389–405.

35. Sled JG, Pike GB. Correction for B(1) and B(0) variations in quantitative T(2) measurements using MRI. Magn Reson Med 2000;43: 589–593.

36. Brey WW, Narayana PA. Correction for intensity falloff in surface coil magnetic resonance imaging. Med Phys 1988;15:241–245.

37. Fan A, Wells WM, Fisher JW, et al. A unified variational approach to denoising and bias correction in MR. Inf Process Med Imaging 2003;18:148–159.